CHEMICAL FRONT PROPAGATION IN PERIODIC FLOWS: FKPP VS G

ALEXANDRA TZELLA* AND JACQUES VANNESTE†

Abstract. We investigate the influence of steady periodic flows on the propagation of chemical fronts in an infinite channel domain. We focus on the sharp front arising in Fisher–Kolmogorov–Petrovskii–Piskunov (FKPP) type models in the limit of small molecular diffusivity and fast reaction (large Péclet and Damköhler numbers, Pe and Da) and on its heuristic approximation by the G equation. We introduce a variational formulation that expresses the two front speeds in terms of periodic trajectories minimizing the time of travel across the period of the flow, under a constraint that differs between the FKPP and G equations. This formulation makes it plain that the FKPP front speed is greater than or equal to the G equation front speed. We study the two front speeds for a class of cellular vortex flows used in experiments. Using a numerical implementation of the variational formulation, we show that the differences between the two front speeds are modest for a broad range of parameters. However, large differences appear when a strong mean flow opposes front propagation; in particular, we identify a range of parameters for which FKPP fronts can propagate against the flow while G fronts cannot. We verify our computations against closed-form expressions derived for Da ≪ Pe and for Da ≫ Pe.

Key words. front propagation, large deviations, WKB, cellular flows, Hamilton–Jacobi, homogenisation, variational principles

AMS subject classifications. Chemically reacting flows (80A32), Combustion (80A25), Hamilton-Jacobi equations (35F21), Approximation methods and numerical treatment of dynamical systems (37M05)

1. Introduction. A classical model for the concentration $\theta(\boldsymbol{x}, t)$ of spreading reacting chemicals is the FKPP, or FK for short, equation named after the classical work by Fisher [18] and Kolmogorov, Petrovskii and Piskunov [25] based on logistic growth and diffusion. Numerous environmental and engineering applications, from the dynamics of ocean plankton to combustion [43, 33], motivate its extension to include the effect of an incompressible background steady flow $\boldsymbol{u}(x, y) = (u, v)$. The FK equation considered here then takes the non-dimensional form

$$\text{(FK)} \qquad \partial_t \theta + \boldsymbol{u} \cdot \nabla \theta = \text{Pe}^{-1} \Delta \theta + \text{Da}\, r(\theta).$$

The reaction term $r(\theta) = \theta(1 - \theta)$ or, more generally, any function $r(\theta)$ that satisfies $r(0) = r(1) = 0$ with $r(\theta) > 0$ for $\theta \in (0, 1)$, $r(\theta) < 0$ for $\theta \notin [0, 1]$ and $r'(0) = \sup_{0 < \theta < 1} r(\theta)/\theta = 1$. The non-dimensional parameters are the Péclet and Damköhler numbers

$$(1.1) \qquad \text{Pe} = VL/\kappa \quad \text{and} \quad \text{Da} = L/(V\tau),$$

where V and L are the characteristic speed and lengthscale of the flow, κ the molecular diffusivity, and τ the reaction time. Motivated by experiments, we focus on two-dimensional channel domains with parallel, impenetrable walls where $v = \partial_y \theta = 0$ and take the front-like initial and boundary conditions

$$\theta(x, y, 0) = \mathbb{1}_{x \le 0}, \quad \theta \to 1 \quad \text{as } x \to -\infty, \quad \theta \to 0 \quad \text{as } x \to \infty,$$

---

*School of Mathematics, University of Birmingham, Edgbaston, Birmingham, B15 2TT, United Kingdom (a.tzella@bham.ac.uk).

†School of Mathematics and Maxwell Institute for Mathematical Sciences, University of Edinburgh, King's Buildings, Edinburgh EH9 3FD, United Kingdom (J.Vanneste@ed.ac.uk).

where $\mathbb{1}$ denotes the indicator function. In the absence of advection, (FK) admits front solutions that propagate from the left to the right of the channel at the non-dimensional 'bare' speed

$$(1.2) \qquad\qquad\qquad c_0 = 2\sqrt{\mathrm{Da}/\mathrm{Pe}}$$

corresponding to the dimensional speed $c_0^* = c_0 V$. When the flow $\boldsymbol{u}(x, y)$ is spatially periodic, front solutions persist as pulsating fronts [47, 48, 4], changing periodically in time as they travel at a speed c_{FK}, so that

$$(1.3) \qquad\qquad \theta\left(x + 2\pi, y, t + 2\pi/c_{\mathrm{FK}}\right) = \theta(x, y, t),$$

where 2π is the spatial period of the flow.

When reaction dominates over diffusion, i.e. when

$$(1.4) \qquad\qquad\qquad \mathrm{Pe}\,\mathrm{Da} \gg 1,$$

the front interface is sharp and can be approximated by a single curve (in 2D as assumed here) where all the reaction takes place. A distinguished regime then arises for

$$(1.5) \qquad\qquad\qquad \mathrm{Da}/\mathrm{Pe} = c_0^2/4 = O(1),$$

when advection and reaction–diffusion both contribute to the front propagation at the same order. In these conditions, a heuristic model is often used in place of (FK). In this model, the front is the zero-level curve $\theta(x, y, t) = 0$, say, where $\theta(x, y, t)$ satisfies the Hamilton–Jacobi equation

$$(\mathrm{G}) \qquad\qquad\qquad \partial_t \theta + \boldsymbol{u} \cdot \nabla\theta = c_0 |\nabla\theta|,$$

termed G equation [46] (see also [41, 23]). This model is popular in the combustion science literature (e.g. [35] and references therein). For $\boldsymbol{u} = \boldsymbol{0}$, the front speed predicted by (G) is obviously c_0, matching the speed predicted by (FK). For spatially periodic $\boldsymbol{u} \neq \boldsymbol{0}$, (G) predicts pulsating front solutions propagating with a speed c_{G} that in general differs from c_{FK} [49, 6]. The relation between the two speeds c_{FK} and c_{G} (with dimensional equivalents $c_{\mathrm{FK}}^* = c_{\mathrm{FK}} V$ and $c_{\mathrm{G}}^* = c_{\mathrm{G}} V$) is the subject of this paper.

Majda and Souganidis [29] showed that in the limit (1.4) the leading-order c_{FK} can be deduced from the long-time solution of a certain Hamilton–Jacobi equation. This long-time solution is obtained by applying the asymptotic procedure of homogenisation [26, 16] which exploits spatial scale separation to express c_{FK} in terms of the eigenvalue of a nonlinear cell problem posed over a single period of the flow. A similar procedure can be applied to (G), leading to a different nonlinear eigenvalue cell problem for c_{G}. The two nonlinear cell problems are significantly simplified for the special case of shear flows [13, 50]. For more general flows and arbitrary c_0 explicit analytical expressions are not available and the two cell problems need to be solved numerically. However, these computations can be rather challenging (see e.g. [24] for the nonlinear cell problem related to c_{FK}). Analytic work has focused on the strong-flow limit corresponding to $c_0 \to 0$ [12, 50, 51].

In this paper, we rely on the variational representation of the two front speeds c_{FK} and c_{G}. For (FK), this approach was introduced by Freidlin and collaborators (see [21, Ch. 10], [19, Ch. 6] and [20]) to establish an expression for c_{FK} in terms of a single trajectory that minimises an action functional. This was subsequently exploited in

[44] to obtain explicit results for cellular flows by carrying out a minimisation over periodic trajectories. For (G), Fermat's principle in a moving medium determines c_{G}. The variational formulations enable us to express c_{FK} and c_{G} in terms of periodic trajectories $\boldsymbol{X}(\tau) = \boldsymbol{X}(0) + (2\pi, 0)$ that minimise the time of travel τ across the period of the flow, under a constraint that differs between (FK) and (G). In both cases, the constraint involves the difference between the velocity of the minimising trajectory and the velocity of the flow. For (FK) the constraint is integral, in terms of the L^2-norm, given by

$$(1.6) \qquad \qquad \tau^{-1} \int_0^\tau |\dot{\boldsymbol{X}}(t) - \boldsymbol{u}(\boldsymbol{X}(t))|^2 \, \mathrm{t} = c_0^2$$

while for (G) the constraint is pointwise and given by

$$(1.7) \qquad \qquad |\dot{\boldsymbol{X}}(t) - \boldsymbol{u}(\boldsymbol{X}(t))|^2 = c_0^2,$$

for all $t \in [0, \tau]$. These formulations allow us to understand the difference between c_{FK} and c_{G}, to immediately deduce that $c_{\mathrm{FK}} \geq c_{\mathrm{G}}$ (already established by [50] using a different approach) and to compute c_{FK} and c_{G} for a large class of steady, periodic $\boldsymbol{u}$.

We begin with the simple case of shear flows $\boldsymbol{u} = (u(y), 0)$ before examining in detail a two-parameter family of periodic cellular flows, given by $\boldsymbol{u} = (-\partial_y \psi, \partial_x \psi)$ with streamfunction

$$(1.8) \qquad \qquad \psi = -Uy - (\sin x + A \sin(2x)) \sin y.$$

This is used as a testbed in numerous experimental studies of advection–diffusion–reaction (e.g., [37, 40, 3, 32, 27]). The classic cellular flow introduced in [38] corresponds to a zero mean velocity $U = 0$ and to $A = 0$. When confined between walls at $y = 0$ and π, this flow consists of a one-dimensional infinite array of periodic cells composed of two vortices of opposite circulation. These vortices are bounded by the separatrix streamline $\psi = 0$ that connects a network of hyperbolic stagnation points (see Fig. 1.1(a)). All streamlines remain closed when $A > 0$ and $U = 0$ but the symmetry $(x, y) \mapsto (x + \pi, \pi - y)$ is broken. For $A > 1/2$, the number of hyperbolic stagnation points doubles and the periodic cell consists of four vortices rotating in alternatively clockwise and anticlockwise directions (see Fig. 1.1(b)). The topology of the streamlines changes drastically for a non-zero mean velocity $U \neq 0$: an open channel, bounded by the separatrices $\psi = 0$ and $\psi = -U\pi$, traverses the domain, splitting apart the row of closed vortices. As the value of $|U|$ increases, the width of the open channel increases (see Fig. 1.1(c) for $U > 0$ and Fig. 1.1(d) for $U < 0$). For $|U|$ large enough, the hyperbolic stagnation points and closed streamlines disappear.

Our aim is to determine the effect of flow structures on the value of the two front speeds c_{FK} and c_{G} and on their difference. To achieve this, we develop and implement a highly accurate numerical method that is based on the efficient discretisation of a pair of variational principles that we obtain. Computations of the two front speeds are complemented by a set of explicit expressions derived by formal asymptotics methods in the limit of small and large values of c_0 and various values of A and U. Table 1.1 summarises the expressions for the basic cellular flow for which $A = U = 0$. These are in agreement with the rigorous bounds developed in [50] for small c_0 (see also [1, 8]).

The paper is organised as follows. In section 2, we provide a brief derivation of the two nonlinear cell problems that determine c_{FK} and c_{G}. In section 3, we introduce the alternative characterisation in the form of a pair of variational principles with
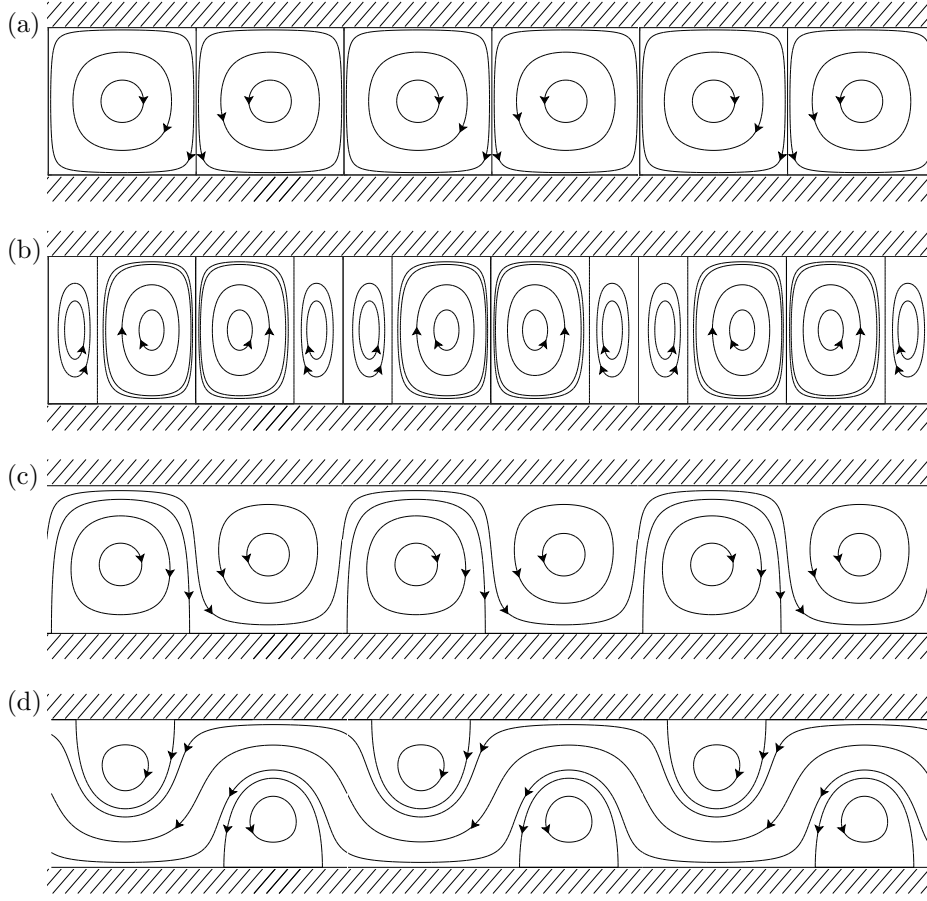
(a)

(b)

(c)

(d)

FIG. 1.1. *Streamlines for the cellular flow with streamfunction (1.8) for (a) $U = 0$, $A = 0$, (b) $U = 0$, $A = 1$, (c) $U = 0.1$, $A = 0$ and (d) $U = -0.5$, $A = 0$. For $U = 0$, all streamlines are closed. When $U \neq 0$, there is a channel of open streamlines.*

constraints (1.6)–(1.7). The two principles greatly simplify for shear flows in which case $c_{\mathrm{FK}} = c_{\mathrm{G}}$. Section 4 is devoted to flows with streamfunction (1.8). The numerical scheme employed for the computations is described in the Appendix. The paper ends with a discussion in section 5.

2. Front speed.

2.1. Equation (FK). Gärtner and Freidlin [22] showed that for initial conditions sufficiently close to a step function, the speed of the front associated with (FK) can be deduced by the long-time behaviour of the solution near the front's leading edge. There $0 < \theta \ll 1$ and $r(\theta) \approx r'(0)\theta = \theta$ so that (FK) becomes

$$(2.1) \qquad \partial_t \theta + \boldsymbol{u} \cdot \nabla \theta = \mathrm{Pe}^{-1} \Delta \theta + \mathrm{Da}\,\theta.$$

For $\mathrm{Pe} \gg 1$ and $\mathrm{Da}/\mathrm{Pe} = c_0^2/4 = O(1)$, the solution can be sought in the WKBJ (Wentzel–Kramers–Brillouin–Jeffreys) or geometric-optics form

$$(2.2) \qquad \theta(\boldsymbol{x}, t) \asymp \mathrm{e}^{-\mathrm{Pe}\,\mathscr{I}(\boldsymbol{x}, t, c_0)}.$$

TABLE 1.1

Asymptotic expressions for the front speed of (FK) and (G) in the basic cellular flow ((1.8) with $A = U = 0$) for small and large 'bare' speed $c_0 = 2\sqrt{\mathrm{Da}/\mathrm{Pe}}$. The difference between the two front speeds is asymptotically small in both limits (see Sec. 4.1 for details). All variables are non-dimensional.

equation	front speed $\sim$	range of validity
(FK)	$\pi/\mathrm{W}_p(32c_0^{-2})$	$c_0 \ll 1$
	$c_0(1 + 3c_0^{-2}/4 - 105c_0^{-4}/64)$	$c_0 \gg 1$
(G)	$-\pi/(2\log(\pi c_0/8))$	$c_0 \ll 1$
	$c_0(1 + 3c_0^{-2}/4 - 109c_0^{-4}/64)$	$c_0 \gg 1$

Collecting the terms with the same powers in Pe, we find that at leading order $\mathscr{I}(\boldsymbol{x}, t, c_0)$ satisfies the Hamilton–Jacobi equation

$$(2.3) \qquad \partial_t \mathscr{I} + \mathscr{H}_{\mathrm{FK}}(\nabla \mathscr{I}, \boldsymbol{x}, c_0) = 0 \quad \text{with} \quad \mathscr{H}_{\mathrm{FK}}(\boldsymbol{p}, \boldsymbol{x}, c_0) = |\boldsymbol{p}|^2 + \boldsymbol{u}(\boldsymbol{x}) \cdot \boldsymbol{p} + c_0^2/4$$

the Hamiltonian. The step-function initial conditions correspond to $\mathscr{I}(\boldsymbol{x}, 0, c_0) = 0$ for $x \leq 0$ and $\mathscr{I}(\boldsymbol{x}, 0, c_0) = \infty$ for $x > 0$, and the boundary conditions to $\partial_y \mathscr{I}(\boldsymbol{x}, t, c_0) = 0$ at $y = 0, \pi$. The front is then identified as the location where (2.2) neither grows nor decays exponentially with time. It is therefore the level curve

$$(2.4) \qquad\qquad\qquad \mathscr{I}(\boldsymbol{x}, t, c_0) = 0.$$

In the long-time limit, the solution to (2.3) converges to that of the homogenised Hamilton–Jacobi equation

$$(2.5) \qquad\qquad\qquad \partial_t \bar{\mathscr{I}} + \bar{\mathscr{H}}_{\mathrm{FK}}(\partial_x \bar{\mathscr{I}}, c_0) = 0.$$

The effective Hamiltonian, $\bar{\mathscr{H}}_{\mathrm{FK}}$, may be derived from a nonlinear eigenvalue problem, obtained by writing the solution to (2.3) as the multiscale expansion

$$(2.6)$$
$$\mathscr{I}(\boldsymbol{x}, t, c_0) = t\left(\mathscr{G}(c, c_0) + t^{-1}\phi(\boldsymbol{x}, c, c_0) + O(t^{-2})\right), \quad \text{where } t \gg 1 \text{ and } c = x/t = O(1).$$

Here c is the slow variable describing the speed of a moving frame of reference and $\boldsymbol{x}$ is the fast variable. We emphasise the particular form of (2.6), with a leading-order term that is independent of $\boldsymbol{x}$ and involves $\mathscr{G}(c, c_0)$ that depends on c only.[1] The next order involves $\phi(\boldsymbol{x}, c, c_0)$ where $\phi(x + 2\pi, y, c, c_0) = \phi(x, y, c, c_0)$ while the boundary conditions at $y = 0, \pi$ imply that there, $\partial_y \phi = 0$. Substituting (2.6) into (2.3) and equating powers of t^{-1} yields at leading order $O(1)$ the nonlinear eigenvalue problem

$$(2.7) \qquad \mathscr{H}_{\mathrm{FK}}((p, 0) + \nabla\phi, \boldsymbol{x}, c_0) = \bar{\mathscr{H}}_{\mathrm{FK}}(p, c_0), \quad \text{where} \quad p = \mathscr{G}'(c, c_0),$$

---

[1]Note that $\mathscr{G}(c, c_0)$ may be interpreted as the Freidlin–Wentzell (small-noise, large-Pe) large-deviation rate function for the position of fluid particles that have been displaced by advection and diffusion to a distance ct in a time $t \gg 1$ (see [21],[19, Ch. 6] and [20] for rigorous treatments).

with the prime denoting derivative with respect to the first argument, can be treated as a parameter and

$$(2.8) \qquad \bar{\mathscr{H}}_{\mathrm{FK}}(p, c_0) = c\,\mathscr{G}'(c, c_0) - \mathscr{G}(c, c_0),$$

is the eigenvalue. It can be shown that $\bar{\mathscr{H}}_{\mathrm{FK}}(p, c_0)$ is unique, non-negative, real and convex in p (see [26, 14] for proofs) and therefore $\bar{\mathscr{H}}_{\mathrm{FK}}(p, c_0)$ and $\mathscr{G}(c, c_0)$ are related via a Legendre transform

$$(2.9) \qquad \mathscr{G}(c, c_0) = \sup_p (p\,c - \bar{\mathscr{H}}_{\mathrm{FK}}(p, c_0)) \quad \text{and} \quad \bar{\mathscr{H}}_{\mathrm{FK}}(p, c_0) = \sup_c (p\,c - \mathscr{G}(c, c_0)).$$

Combining (2.4) with (2.6) gives the front speed c_{FK} as the solution of

$$(2.10) \qquad \mathscr{G}(c_{\mathrm{FK}}, c_0) = 0,$$

with $c_{\mathrm{FK}} > 0$ corresponding to (FK) fronts that propagate from left to right. Using (2.9) it can be expressed explicitly in terms of the effective Hamiltonian $\bar{\mathscr{H}}(p)$ as

$$(2.11) \qquad c_{\mathrm{FK}} = \inf_p \frac{1}{p} \bar{\mathscr{H}}_{\mathrm{FK}}(p, c_0),$$

an expression first obtained in [29].

2.2. Equation (G). The long-time solution to equation (G) can be treated similarly. It satisfies the homogenised Hamilton–Jacobi equation

$$(2.12) \qquad \partial_t \bar{\theta} + \bar{\mathscr{H}}_{\mathrm{G}}(\partial_x \bar{\theta}, c_0) = 0,$$

with an effective Hamiltonian $\bar{\mathscr{H}}_{\mathrm{G}}$ found as eigenvalue of the nonlinear cell problem

$$(2.13) \qquad \mathscr{H}_{\mathrm{G}}((p, 0) + \nabla\phi, \boldsymbol{x}, c_0) = \bar{\mathscr{H}}_{\mathrm{G}}(p, c_0),$$

where

$$(2.14) \qquad \mathscr{H}_{\mathrm{G}}(\boldsymbol{p}, \boldsymbol{x}, c_0) = \boldsymbol{u}(\boldsymbol{x}) \cdot \boldsymbol{p} - c_0|\boldsymbol{p}|.$$

Note that the nonlinearity $|\boldsymbol{p}|^2$ in $\mathscr{H}_{\mathrm{FK}}$ is replaced here by $|\boldsymbol{p}|$. Nevertheless, $\bar{\mathscr{H}}_{\mathrm{G}}$ is unique and convex (details and proofs can be found in [49, 7]). The solution of (2.12) is then $\bar{\theta} = t\mathscr{F}(c, c_0)$ where $\mathscr{F}(c, c_0)$ and $\bar{\mathscr{H}}_{\mathrm{G}}(p, c_0)$ and are related via a Legendre transform analogous to (2.9). Since the front corresponds to $\theta(\boldsymbol{x}, t) = 0$, in the long-time limit, the speed c_{G} of right-propagating (G) fronts is found as the positive solution of $\mathscr{F}(c_{\mathrm{G}}, c_0) = 0$ or, equivalently, as

$$(2.15) \qquad c_{\mathrm{G}} = \inf_p \frac{1}{p} \bar{\mathscr{H}}_{\mathrm{G}}(p, c_0).$$

We now obtain alternative formulations to (2.11) and (2.15) that shed light on the difference between the two speeds, are amenable to straightforward numerical computations, and yield explicit expressions in asymptotic limits.

3. Variational principles.

3.1. Equation (FK). It is well known (see e.g. [15]) that the solution to (2.3) may be written as a variational principle involving an action functional associated with the Lagrangian

$$(3.1) \qquad \mathscr{L}(\dot{\boldsymbol{X}}, \boldsymbol{X}) = \frac{1}{4}|\dot{\boldsymbol{X}} - \boldsymbol{u}(\boldsymbol{X})|^2$$

that is dual to the Hamiltonian $\mathscr{H}_{\mathrm{FK}}$ in (2.3). For $x > 0$ the solution is given by

$$(3.2) \qquad \mathscr{I}(\boldsymbol{x}, T, c_0) = \frac{1}{4}\left(\inf_{\boldsymbol{X}(\cdot)} \int_0^T |\dot{\boldsymbol{X}}(t) - \boldsymbol{u}(\boldsymbol{X}(t))|^2 \, \mathrm{t} - c_0^2 T \right),$$

$$(3.3) \qquad\qquad\qquad \text{subject to } \boldsymbol{X}(0) = (0, \cdot), \quad \boldsymbol{X}(T) = \boldsymbol{x},$$

where $\boldsymbol{X}(\cdot)$ represents a family of smooth trajectories with $Y(\cdot) \in [0, \pi]$. From (2.6) we have

$$(3.4) \qquad \mathscr{G}(c, c_0) = \lim_{T \to \infty} \frac{\mathscr{I}((cT, y), T, c_0)}{T},$$

where the dependence on the specific value of y drops out (e.g. [36]). Together with (3.2) this determines the function $\mathscr{G}(c, c_0)$.

Expression (3.4) can be simplified using the spatial periodicity of the background velocity $\boldsymbol{u}$ [44]. Assuming that the minimising trajectory inherits inherits the same spatial periodicity, we take $T = n\tau$ with $\tau = 2\pi/c$ and $n \gg 1$ to reduce (3.4) to

$$(3.5) \qquad \mathscr{G}(c, c_0) = \frac{1}{4}\left(\frac{1}{\tau} \inf_{\boldsymbol{X}(\cdot)} \int_0^\tau |\dot{\boldsymbol{X}}(t) - \boldsymbol{u}(\boldsymbol{X}(t))|^2 \, \mathrm{t} - c_0^2 \right),$$

$$\text{subject to } \boldsymbol{X}(\tau) = \boldsymbol{X}(0) + (2\pi, 0).$$

Expression (3.5) provides a direct way to compute the minimising trajectory and, from (2.10), the corresponding front speed c_{FK}, both numerically and in asymptotic limits. Such computations were carried out in [44] for the specific case of the cellular flow with closed streamlines that we consider further in Section 4. These computations were validated against the numerical evaluation of c_{FK} for finite Péclet and Damköhler numbers obtained from an advection–diffusion eigenvalue problem and direct numerical simulations of (FK) with $r(\theta) = \theta(1 - \theta)$.

We now obtain an alternative variational characterisation of c_{FK}. Since c_{FK} satisfies $\mathscr{G}(c_{\mathrm{FK}}, c_0) = 0$, it can be written as extremum of the function

$$(3.6) \qquad S(\lambda) = \sup_\tau \frac{2\pi}{\tau} - \lambda \mathscr{G}\left(\frac{2\pi}{\tau}, c_0 \right),$$

for arbitrary variations of the Lagrange multiplier λ. Here we use that $\mathscr{G}$ is convex in c, so that a single $\tau = \tau_{\mathrm{FK}}$ satisfies the constraint $\mathscr{G}(2\pi/\tau, c_0) = 0$ enforced by λ. Using (3.5) and redefining λ to absorb a factor $1/4$, we can rewrite this as

$$(3.7) \qquad S(\lambda) = \sup_\tau \sup_{\boldsymbol{X}(\cdot)} \left(\frac{2\pi}{\tau} - \lambda \left(\frac{1}{\tau} \int_0^\tau |\dot{\boldsymbol{X}}(t) - \boldsymbol{u}(\boldsymbol{X}(t))|^2 \mathrm{t} - c_0^2 \right) \right),$$

$$(3.8) \qquad\qquad\qquad \text{subject to } \boldsymbol{X}(\tau) = \boldsymbol{X}(0) + (2\pi, 0).$$

This can be interpreted as the maximisation of $2\pi/\tau$ under a constraint enforced by the Lagrange multiplier λ. Therefore, the front speed predicted by (FK) for Pe, Da $\gg 1$, $c_0 = O(1)$ is given as

$$(3.9) \qquad c_{\mathrm{FK}} = \frac{2\pi}{\tau_{\mathrm{FK}}}, \quad \text{where} \quad \tau_{\mathrm{FK}} = \inf_{\boldsymbol{X}(\cdot)} \tau, \quad \text{subject to} \quad \boldsymbol{X}(\tau) = \boldsymbol{X}(0) + (2\pi, 0)$$

$$\text{and} \ \frac{1}{\tau} \int_0^\tau |\dot{\boldsymbol{X}}(t) - \boldsymbol{u}(\boldsymbol{X}(t))|^2 \mathrm{d}t = c_0^2.$$

This variational characterisation expresses c_{FK} as the maximum mean velocity achievable by periodic trajectories that are constrained to depart from passive-particle trajectories in a prescribed way.

3.2. Equation (G). An analogous variational characterisation describes the front speed associated with (G). Taking the same initial conditions as for (FK), the front propagates from its initial location at $\boldsymbol{X}(0) = (0, \cdot)$ along trajectories $\boldsymbol{X}(t)$ that obey Fermat's principle in a moving medium (e.g. [9], Vol. 1, Sec. IV.1). Thus the front reaches location $\boldsymbol{x}$ after a travel time

$$(3.10) \qquad \mathscr{T}(\boldsymbol{x}, c_0) = \inf_{\boldsymbol{X}(\cdot)} T \quad \text{with} \quad \boldsymbol{X}(0) = (0, \cdot), \ \boldsymbol{X}(T) = \boldsymbol{x},$$

$$\text{subject to} \ |\dot{\boldsymbol{X}}(t) - \boldsymbol{u}(\boldsymbol{X}(t))|^2 = c_0^2 \ \text{for} \ t \in [0, T],$$

where again we assume that $\boldsymbol{X}(\cdot)$ represents a family of smooth trajectories with $Y(\cdot) \in [0, \pi]$. In the long-time limit, x is large and the front moves at a constant speed given by

$$(3.11) \qquad c_{\mathrm{G}} = \lim_{x \to \infty} \frac{x}{\mathscr{T}((x, y), c_0)},$$

where once more the dependence on y drops out. This characterisation is significantly simplified if we apply the same strategy as before and assume that the minimising trajectory is periodic. Taking $T = n\tau$ with $n \gg 1$, we obtain that

$$(3.12) \qquad c_{\mathrm{G}} = \frac{2\pi}{\tau_{\mathrm{G}}}, \quad \text{where} \quad \tau_{\mathrm{G}} = \inf_{\boldsymbol{X}(\cdot)} \tau, \quad \text{subject to} \quad \boldsymbol{X}(\tau) = \boldsymbol{X}(0) + (2\pi, 0)$$

$$\text{and} \ |\dot{\boldsymbol{X}}(t) - \boldsymbol{u}(\boldsymbol{X}(t))|^2 = c_0^2 \ \text{for} \ t \in [0, \tau].$$

This characterisation of the front speed for (G) closely parallels the characterisation (3.9) of the front speed for (FK).

For practical computations, it is convenient to rewrite (3.12) taking x as the independent variable, using

$$(3.13) \qquad \frac{dt}{dx} = T'(x), \quad \text{with} \quad T(0) = 0,$$

where $T(x)$ denotes the time it takes to reach the point $(x, Y(x))$. The minimal travel time over a spatial period is then expressed as

$$(3.14) \ c_{\mathrm{G}} = \frac{2\pi}{\tau_{\mathrm{G}}}, \quad \text{where} \ \tau_{\mathrm{G}} = \inf_{T(\cdot), Y(\cdot)} \int_0^{2\pi} T'(x) \mathrm{d}x \quad \text{subject to} \ Y(2\pi) = Y(0)$$

$$\text{and} \ |T'(x)^{-1}(1, Y'(x)) - \boldsymbol{u}(x, Y(x))|^2 = c_0^2 \ \text{for} \ x \in [0, 2\pi],$$

and $Y(\cdot)$, $T(\cdot)$ are taken to be smooth.

3.3. Comparison. We now compare the two variational characterisations (3.9) and (3.12) for the (FK) and (G) equations. In both the front speeds are expressed in terms of the travel times τ_{FK} and τ_{G} which are determined by the periodic trajectories that traverse a spatial period of the flow in the least time. The only difference is that the pointwise constraint on the relative velocity in (3.12) is replaced by a slacker, time-averaged constraint in (3.9). An immediate consequence is that

$$(3.15) \qquad\qquad c_{\mathrm{FK}} \geq c_{\mathrm{G}},$$

The same result was obtained in [50] using a min-max formulation of (2.7) and (2.13).

While (3.9) and (3.12) are useful for comparisons of this type, for numerical computations we found it convenient to use (3.5) and (3.14) instead. Eq. (3.5) is useful for (FK) when, as is the case in section 4, we are interested in computing c_{FK} for a range of values of c_0: the simple dependence of $\mathscr{G}$ on c_0 means that the condition $\mathscr{G}(c_{\mathrm{FK}}, c_0) = 0$ gives an explicit variational formula for c_0 as a function of c_{FK} with the endpoint condition as sole constraint.

The variational characterisation (3.12) is also useful to establish a necessary condition for the existence of right-propagating front solutions for the (G) equation. It is easy to see from the constraint in (3.12) that

$$(3.16) \qquad\qquad c_{\mathrm{G}} > 0 \quad \text{implies} \quad c_0 > -\min_x \max_y u(x, y).$$

For smaller c_0, there are no right-propagating (G) fronts. From (3.15) we then expect that, for a range of c_0, there exist right-propagating fronts for (FK) but not for (G). We provide explicit examples confirming this in section 4.3.

Shear flows. It is easy to show that for shear flows with velocity $\boldsymbol{u}(\boldsymbol{x}) = (u(y), 0)$, $c_{\mathrm{FK}} = c_{\mathrm{G}}$. For (FK), the Euler–Lagrange equations associated with the functional in (3.5) can be written as

$$(3.17) \qquad \dot{X}(t) - u(Y(t)) = A_1, \quad \tfrac{1}{2}\dot{Y}^2(t) + A_1 u(Y(t)) = A_2,$$

where A_1 and A_2 are two constants. The minimum of the functional is then achieved when $Y(t) = Y_0$, where Y_0 is a constant to be determined. It follows that $\dot{X}(t) = \text{const} = c$ as imposed by the endpoint condition. The functional then reduces to $(c - u(Y_0))^2$. Its minimum is non zero for $c > u_+ = \max_y u(y)$, the maximum velocity in the channel, and given by $(c - u_+)^2$ with $Y_0 = Y_+$ such that $u(Y_+) = u_+$. Thus,

$$(3.18) \qquad \mathscr{G}(c, c_0) = \left((c - u_+)^2 - c_0^2\right)/4 \quad \text{for} \quad c > u_+,$$

and solving (2.10) gives the front speed $c_{\mathrm{FK}} = c_0 + u_+$.

On the other hand, the pointwise constraint (3.12) of the velocity may be parameterised so that

$$(3.19) \qquad \dot{X}(t) = u(Y(t)) + c_0 \cos\Theta(t) \quad \text{and} \quad \dot{Y}(t) = c_0 \sin\Theta(t),$$

where $\Theta(t)$ has the same period as $\boldsymbol{X}(t)$. The minimum value of τ is obtained by maximising $\dot{X}(t)$. This is achieved for $\dot{Y}(t) = 0$, $\Theta(t) = 0$ and $Y = Y_+$, i.e. for trajectories that follow the (straight) streamline associated with maximal flow velocity. We deduce that

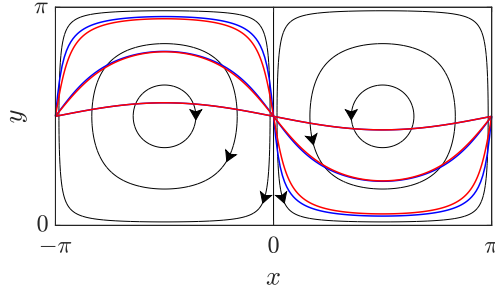$$(3.20) \qquad\qquad c_{\mathrm{FK}} = c_{\mathrm{G}} = c_0 + u_+.$$

FIG. 4.1. *(Color online). Streamlines (thin black lines) of the closed cellular flow with stream-function (1.8) and $U = A = 0$. and corresponding periodic trajectories for (FK) (minimising (3.9), thick blue lines) and (G) (minimising (3.12), thick red lines) obtained numerically for $c_0 = 0.1$, $c_0 = 1$ and $c_0 = 10$. The trajectories become closer to the straight line $y = \pi/2$ as c_0 increases at which point the difference between the two sets of trajectories is minimal.*

We therefore conclude that (FK) and (G) are equivalent in describing the long-time speed of propagation. This was previously argued to be the case in [2], can be inferred from the analysis in [13] and was proved in [50]. It is clear that a right-propagating front is obtained for both (FK) and (G) provided that $c_0 > -u_+$, and that the front is stationary for $c_0 = -u_+ > 0$.

4. Front speeds for periodic flows. For more general flows, closed-form formulas are not available. We use the variational problems (3.5) and (3.14) whose solutions are easy to approximate numerically. We obtain numerical approximations by discretising trajectories, action functional and constraints and determining the optimal solutions by minimisation. The numerical procedure is detailed in Appendix A. We use this procedure to compute the front speeds for (FK) and (G) and a range of two-dimensional periodic flows. We now describe the results.

4.1. Cellular flow. We first compute the solutions for the closed cellular flow with streamfunction (1.8) and $U = A = 0$. Figure 4.1 shows characteristic examples of minimising trajectories obtained for three different values of c_0. For large values of c_0, the periodic trajectories for (FK) and (G) are close to the straight line $y = \pi/2$. In this case, the two trajectories are practically indistinguishable. A larger difference is obtained for small values of c_0, in which case both trajectories follow closely a streamline near the separatrix $\psi = 0$. In all cases it is clear that the trajectories are invariant under the transformations $(x, y) \mapsto (-x, \pi - y)$ and $(x, y) \mapsto (x + \pi, \pi - y)$.

Figure 4.2 shows the behaviour of the front speeds for (FK) and (G) as a function of c_0. Clearly, there is a difference between c_{FK} and c_{G} which is more marked for smaller values of c_0. However, this difference is small: (G) only slightly underpredicts the front speed of (FK). The behaviour of c_{FK} and c_{G} and their difference can be captured by explicit expressions obtained in two asymptotic limits.

4.1.1. Small-c_0 asymptotics. The first asymptotic limit corresponds to $c_0 \ll 1$. This limit has been studied in [50] who rigorously derived tight bounds on c_{FK} and c_{G}. We find an approximation to c_{FK} by approximating $\mathscr{G}(c, c_0)$ in (3.5) for $c \ll 1$. We previously found [44] that the minimising periodic trajectory in (3.5) may be divided into two regions that we now describe. In region I, $X(t) \ll 1$ and therefore we may seek a regular expansion in powers of c of the form

$$(4.1) \qquad \boldsymbol{X}(t) = (0, Y_0(t)) + c(X_1(t), Y_1(t)) + \cdots,$$

where, without loss of generality, we take $X(0) = 0$. In region II, $Y(t) \ll 1$ and so we take

(4.2) $$\bar{\boldsymbol{X}}(t) = (\bar{X}_0(t), 0) + c(\bar{X}_1(t), \bar{Y}_1(t)) + \cdots,$$

where $\bar{X}(\tau/4) = \pi/2$ with $\tau = 2\pi/c$. We then exploit the symmetries that characterises the streamfunction to extend the trajectory over the whole time period τ.

Substituting (4.1) and (4.2) into (3.5) gives a sequence of integrals corresponding to successive powers of c. Minimising each yields

(4.3a) $$\dot{Y}_0 = -\sin Y_0, \;\; \ddot{X}_1 = X_1, \;\; \dot{Y}_1 = -Y_1 \cos Y_0,$$

(4.3b) $$\dot{\bar{X}}_0 = \sin \bar{X}_0, \;\; \dot{\bar{X}}_1 = \bar{X}_1 \cos X_0, \;\; \dot{\bar{Y}}_1 = -\bar{Y}_1 \cos \bar{X}_0.$$

Thus at $O(c)$ in Region II, the minimising trajectory follows exactly the streamlines. The two solutions can be matched in their common region of validity, given by $X(t), Y(t) \ll 1$ (and corresponding to $1 \ll t \ll \tau/4$), to obtain

(4.4a) $\quad X_1(t) = 4\,e^{-\tau/4} \sinh t\,/c, \;\; Y_0(t) = 2\tan^{-1}(e^{-t}), \;\; Y_1(t) = 0,$

(4.4b) $\quad \bar{X}_0(t) = 2\tan^{-1}(e^{-\tau/4+t}), \;\; \bar{X}_1(t) = 0, \;\; \bar{Y}_1(t) = 4\,e^{-\tau/4} \cosh(\tau/4 - t)\,/c.$

At this order, the only non-zero contribution to the integral in (3.5) comes from the behaviour in Region I. We use (4.4a) to obtain that $|\dot{\boldsymbol{X}}(t) - \boldsymbol{u}(\boldsymbol{X}(t))|^2 \sim c^2(\dot{X}_1(t) - X_1(t) \cos Y_0(t))^2$ and thus

(4.5) $$\mathscr{G}(c, c_0) \sim \frac{1}{4}\left(\frac{32}{\pi} c e^{-\pi/c} - c_0^2\right)$$

since $c = 2\pi/\tau$. Solving $\mathscr{G}(c_{\mathrm{FK}}, c_0) = 0$ finally gives the approximation

(4.6) $$c_{\mathrm{FK}} \sim \frac{\pi}{\mathrm{W}_p\left(32 c_0^{-2}\right)} \qquad \text{for} \;\; c_0 \ll 1.$$

Here, W_p is the principal branch of the Lambert W function [10]. The above results were previously derived in [44] and included here for completeness. It is consistent with the bounds of [50].

We obtain an approximation for c_{G} in a similar way. The periodic trajectory associated with the variational principle (3.12) are divided into the same two regions as above. The regular expansions are this time more naturally expressed in powers of c_0 so that in region I where $X(t) \ll 1$, we take

(4.7) $$\boldsymbol{X}(t) = (0, Y_0(t)) + c_0(X_1(t), Y_1(t)) + \cdots,$$

where $X(0) = 0$. In region II, $Y(t) \ll 1$ and so we take

(4.8) $$\bar{\boldsymbol{X}}(t) = (\bar{X}_0(t), 0) + c_0(\bar{X}_1(t), \bar{Y}_1(t)) + \cdots,$$

where $\bar{X}(\tau/4) = \pi/2$ and once more extend the behaviour over the whole τ using symmetry.

The periodic trajectory is now obtained by substituting (4.7) and (4.8) inside the pointwise constraint in (3.12) from where we obtain equations for each power of c_0. This leads to two sets of equations

(4.9a) $\quad \dot{Y}_0 = -\sin Y_0, \;\; \dot{X}_1 = X_1 \cos Y_0 + \cos \Theta_0, \;\; \dot{Y}_1 = -Y_1 \cos Y_0 + \sin \Theta_0,$

(4.9b) $\quad \dot{\bar{X}}_0 = \sin \bar{X}_0, \;\; \dot{\bar{X}}_1 = \bar{X}_1 \cos \bar{X}_0 + \cos \bar{\Theta}_0, \;\; \dot{\bar{Y}}_1 = -\bar{Y}_1 \cos \bar{X}_0 + \sin \bar{\Theta}_0,$
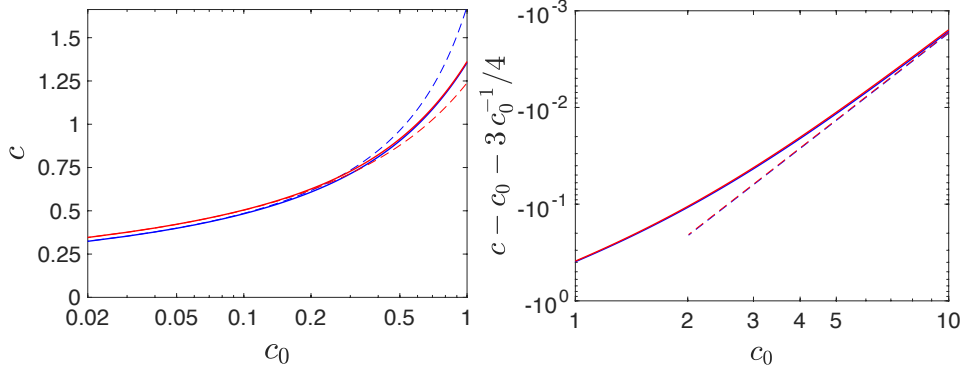
Fɪɢ. 4.2. *(Color online). Comparison between numerical and asymptotic results of the front speed c associated with equations (G) (in blue) and (FK) (in red). The numerical results are derived from the minimisation of (3.9) (solid blue line) and (3.12) (solid red line). These are juxtaposed against (left) the small-c_0 approximations (4.6) (dashed blue line) and (4.11) (dashed red line) and (right) the large-c_0 approximations (4.15) (dashed blue line) and (4.18) (dashed red line).*

where $\Theta_0(t)$ and $\bar{\Theta}_0(t)$ arise when parameterising the constraint (3.12) in polar coordinates. The minimum value of τ, denoted by τ_{G}, is obtained by maximising $\dot{X}_1(t)$, $\dot{\bar{X}}_0(t)$ and $\dot{\bar{X}}_1(t)$. This gives $\Theta_0(t) = \bar{\Theta}_0(t) = 0$ and leads to

(4.10a)
$$X_1(t) = 2\cosh t \, \tan^{-1}(\tanh(t/2)), \quad Y_0(t) = 2\tan^{-1}(e^{-t}), \quad Y_1(t) = 0,$$

(4.10b)
$$\bar{X}_0(t) = 2\tan^{-1}(e^{-\tau_{\mathrm{G}}/4+t}), \quad \bar{X}_1(t) = -\tanh(\tau_{\mathrm{G}}/4-t), \quad \bar{Y}_1(t) = \alpha\cosh(\tau_{\mathrm{G}}/4-t),$$

since $c_{\mathrm{G}} = 2\pi/\tau_{\mathrm{G}}$, where α is a constant to be determined. Matching between the solutions at $O(c_0)$ in their common region of validity, given by $X(t), Y(t) \ll 1$ (the same cell corner as above), yields an expression for c_{G}. Using (3.12), we deduce that

(4.11)
$$c_{\mathrm{G}} = -\frac{\pi}{2\log(\pi c_0/8)}\left(1 + O(c_0^2)\right), \quad \text{for} \quad c_0 \ll 1$$

and $\alpha = \pi/2$. The order of the error is estimated by matching the solutions at $O(c_0^2)$ (calculations not shown). This is qualitatively similar to the expression obtained in [1, 8] using a heuristic approach and consistent with the rigorous bounds of [50].

Figure 4.2 shows that expressions (4.6) and (4.11) are in excellent agreement with our numerical solutions; the same is true for expressions (4.4) and (4.10) describing the trajectories (not shown). We may use $W_p(x) = \log(x) - \log\log(x) + o(1)$ as $x \to \infty$ to further approximate (4.6) as $c_{\mathrm{FK}} \sim -\pi/\left(2\log(c_0/\sqrt{32})\right)$. This approximation highlights the leading-order difference between (4.6) and (4.11). However, this is only a rough approximation which cannot, for instance, capture the non-monotonic behaviour of $c_{\mathrm{FK}} - c_{\mathrm{G}}$ that arises for small c_0 values (not shown). Note that both derivations of (4.6) and (4.11) tacitly assume that $Y_0(0) = \pi/2$. This is easily shown to be the case once the behaviour of the trajectory over the whole (rather than a quarter) spatial period of the flow is taken into account.

4.1.2. Large-c_0 asymptotics. A second asymptotic limit corresponds to $c_0 \gg 1$. We extend the approach in [44] and take the minimising trajectory associated

with the functional in (3.5) to be at leading order a straight line with higher order corrections given by a regular expansion in c^{-1}:

$$(4.12) \quad \boldsymbol{X}(t) = (ct, Y_0) + c^{-1}(X_1, Y_1) + c^{-2}(X_2, Y_2) + c^{-3}(X_3, Y_3) + c^{-4}(X_4, Y_4) + \cdots,$$

where $X(0) = 0$ and $Y(0) = Y_0$. Here, Y_0 is a constant and $X_i(ct)$ and $Y_i(ct)$ are 2π-periodic functions (with zero mean). Substituting (4.12) into (3.5) gives a sequence of integrals corresponding to successive powers of c^{-1}, obtained using a symbolic algebra package. These are in turn minimised up to $O(c^{-2})$ with respect to Y_0, $X_1(ct)$, $Y_1(ct)$, $X_2(ct)$ and $Y_2(ct)$ (contributions from $X_3(ct)$, $Y_3(ct)$, $X_4(ct)$ and $Y_4(ct)$ cancel) yielding

$$(4.13) \qquad Y_0 = \pi/2, \ \ X_1 = Y_2 = 0, \ \ Y_1 = -2\sin(ct), \ \ X_2 = -\frac{3}{8}\sin(2ct).$$

Introducing (4.13) into (3.5) we obtain

$$(4.14) \qquad \mathscr{G}(c, c_0) = \frac{1}{4}\left(c^2 - \frac{3}{2} + \frac{87}{32}c^{-2} - c_0^2\right) + O(c^{-4}),$$

after a few manipulations. This leads to the asymptotics of the speed

$$(4.15) \qquad c_{\text{FK}} = c_0\left(1 + \frac{3}{4}c_0^{-2} - \frac{105}{64}c_0^{-4} + O(c_0^{-6})\right) \qquad \text{for } c_0 \gg 1,$$

with the first two terms previously derived in [44].

In a similar manner, the minimising trajectory associated with the variational principle (3.12) for (G) is at leading order a straight line. Using the alternative variational characterisation (3.14), we write the trajectory in terms of x and take a regular expansion in powers of c_0^{-1}:

$$(4.16a) \qquad T(x) = c_0^{-1}(x + c_0^{-1}T_1 + c_0^{-2}T_2 + c_0^{-3}T_3 + c_0^{-4}T_4) + \cdots,$$

$$(4.16b) \qquad Y(x) = Y_0 + c_0^{-1}Y_1 + c_0^{-2}Y_2 + c_0^{-3}Y_3 + c_0^{-4}Y_4 + \cdots,$$

where $Y(0) = Y_0$. The Y_i's are 2π-periodic functions satisfying $Y_i(0) = 0$ while $T_i(0) = 0$ for all $i \geq 1$. We substitute these inside the pointwise constraint in (3.14) from where we obtain equations for each power of c_0^{-1}. This leads to expressions for $T_i'(x)$ which are in turn used to minimise $\int_0^{2\pi} T_i' \, \mathrm{x}$. Up to $O(c_0^{-2})$ and after a few manipulations carried out with a symbolic algebra package we obtain that

$$(4.17a) \qquad T_1 = T_3 = 0, \ \ T_2 = -3x/4 + f(x), \ \ T_4(x) = 145x/64 + g(x),$$

$$(4.17b) \qquad Y_0 = \pi/2, \ \ Y_1 = -2\sin x, \ \ Y_2 = 0,$$

where $f(x) = 5\sin(2x)/8$ and $g(x) = -Y_3(x)\cos x - 143\sin(2x)/96 + 17\sin(4x)/768$ are 2π-periodic and therefore do not contribute to the value of τ_{G}. Note that the difference between the two trajectories obtained in (4.13) and (4.17) only appears at $O(c_0^{-2})$. We finally use (3.14) to deduce that

$$(4.18) \qquad c_{\text{G}} = c_0\left(1 + \frac{3}{4}c_0^{-2} - \frac{109}{64}c_0^{-4} + O(c_0^{-6})\right) \qquad \text{for } c_0 \gg 1.$$

Comparing expressions (4.15) and (4.18) confirms that the difference between the front speeds for the (FK) and (G) equation is very small: equation (G) only slightly underpredicts the front speed. This is confirmed in Figure 4.2 which focuses on verifying (4.15) and (4.18). It is clear that the two approximations (4.15) and (4.18) are in excellent agreement with the numerical results; however, they are too close apart to distinguish.
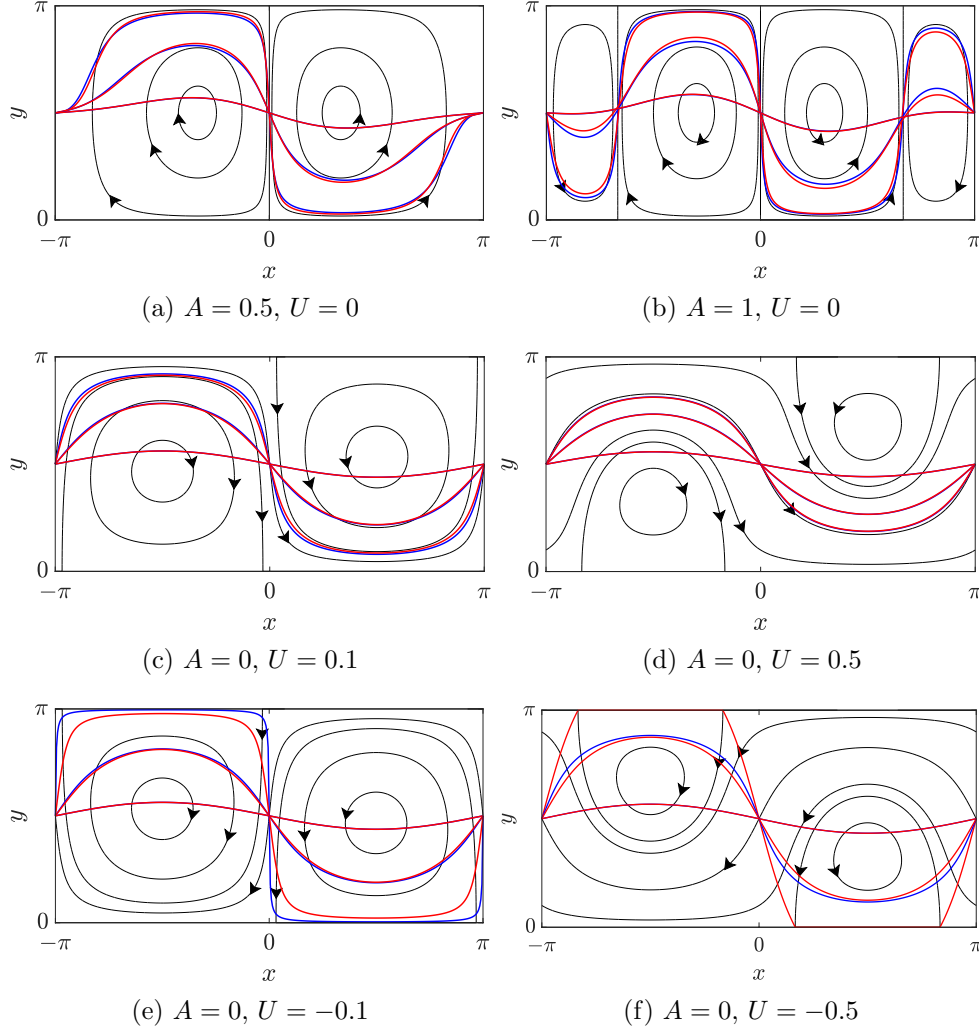
(a) $A = 0.5$, $U = 0$

(b) $A = 1$, $U = 0$

(c) $A = 0$, $U = 0.1$

(d) $A = 0$, $U = 0.5$

(e) $A = 0$, $U = -0.1$

(f) $A = 0$, $U = -0.5$

FIG. 4.3. *(Color online). Streamlines (thin black lines) of the closed cellular flow with stream-function (1.8) with $A \neq 0$ and $U = 0$ (top row) and with $A = 0$ and $U \neq 0$ (middle and bottom rows), and corresponding periodic trajectories for (FK) (minimising (3.9), thick blue lines) and (G) (minimising (3.12), thick red lines). For the top and middle rows, the minimising trajectories are plotted for $c_0 = 0.1$, 1 and 10 (cf. Figure 4.1 for $A = U = 0$). For panel (e), with $U = -0.1$, there is no right-propagating (G) front for $c_0 = 0.1$ and the three values $c_0 = 0.11$, 1 and 10 have been used. For panel (f), with $U = -0.5$, there are no right-propagating (FK) and (G) fronts for $c_0 = 0.01$ and the values $c_0 = 0.19$, 1 and 10 have been used; there is no right-propagating (G) front for $c_0 = 0.19$. Note that the (FK) and (G) trajectories are often indistinguishable for the larger values of c_0.*

4.2. Perturbed cellular flow. We now investigate the effect of perturbing the basic cellular flow by taking for $A \neq 0$ in the streamfunction (1.8), keeping $U = 0$. The perturbation breaks a symmetry of the streamfunction. Characteristic examples of trajectories associated with (FK) and (G) are shown in Figure 4.3 (top row) for two values of A corresponding to distinctly different flow topologies. The trajectories remain symmetric for the transformation $(x, y) \mapsto (-x, \pi - y)$. Qualitatively, they are similar to those obtained for $A = 0$, following closely the straight line $y = \pi/2$
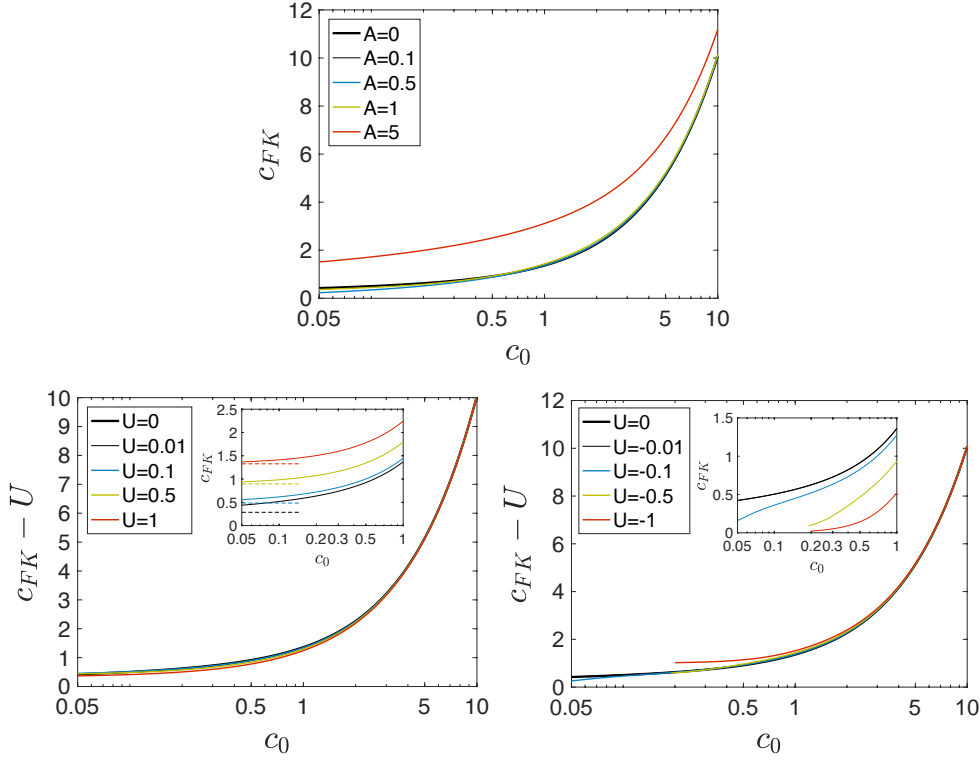
FIG. 4.4. *(Color online). Front speed c_{FK} associated with equation (FK) plotted as a function of the bare speed c_0 for the flow with streamfunction (1.8) for (top row) various values of A with $U = 0$ and (bottom row) for various values of U with $A = 0$ (c_{FK} is shifted by U). The insets focus on the small-c_0 behaviour of c_{FK} (solid lines) and (left) how this compares with $c_+(U)$ obtained from (4.19) (dashed lines).*

when c_0 is large and the separatrix when c_0 is small. Despite the more complex flow structure, the difference between the (FK) and (G) trajectories remains small.

Figure 4.4 (top) shows the behaviour of c_{FK} as a function of c_0. For $0 < A \leq 1$, the value of c_{FK} does not greatly differ from the corresponding value obtained for $A = 0$. A significant difference is obtained for $A = 5$. For large c_0, c_{FK} increases quadratically with A. This can be shown by generalising the asymptotic result (4.15) to find, after a lengthy computation, that $c_{\mathrm{FK}} = c_0(1 + (12 + 9A^2)c_0^{-2}/16 - 3(280 + 504A^2 + 101A^4)c_0^{-4}/512 + \cdots)$ for $c_0 \gg 1$ and $A = o(c_0)$. Expansions (4.1) and (4.2) can in principle also be generalised to provide an explicit expression for c_{FK} when $c_0 \ll 1$. However, the computation becomes very involved, especially for $A \geq 1/2$ when the number of hyperbolic stagnation points is doubled; we have not attempted this computation.

Figure 4.5 (top left) shows the difference between the two front speeds c_{FK} and c_{G} as a function of c_0 and for a number of values of A. This varies non-monotonically with c_0, with a peak whose location is not simply related to A. We observe that for values of c_0 as large as 1, there is no clear relation between this difference and the value of A. For larger values of c_0, the difference increases with A. This can be shown using the generalisations of the asymptotic approximations (4.15) and (4.18) which
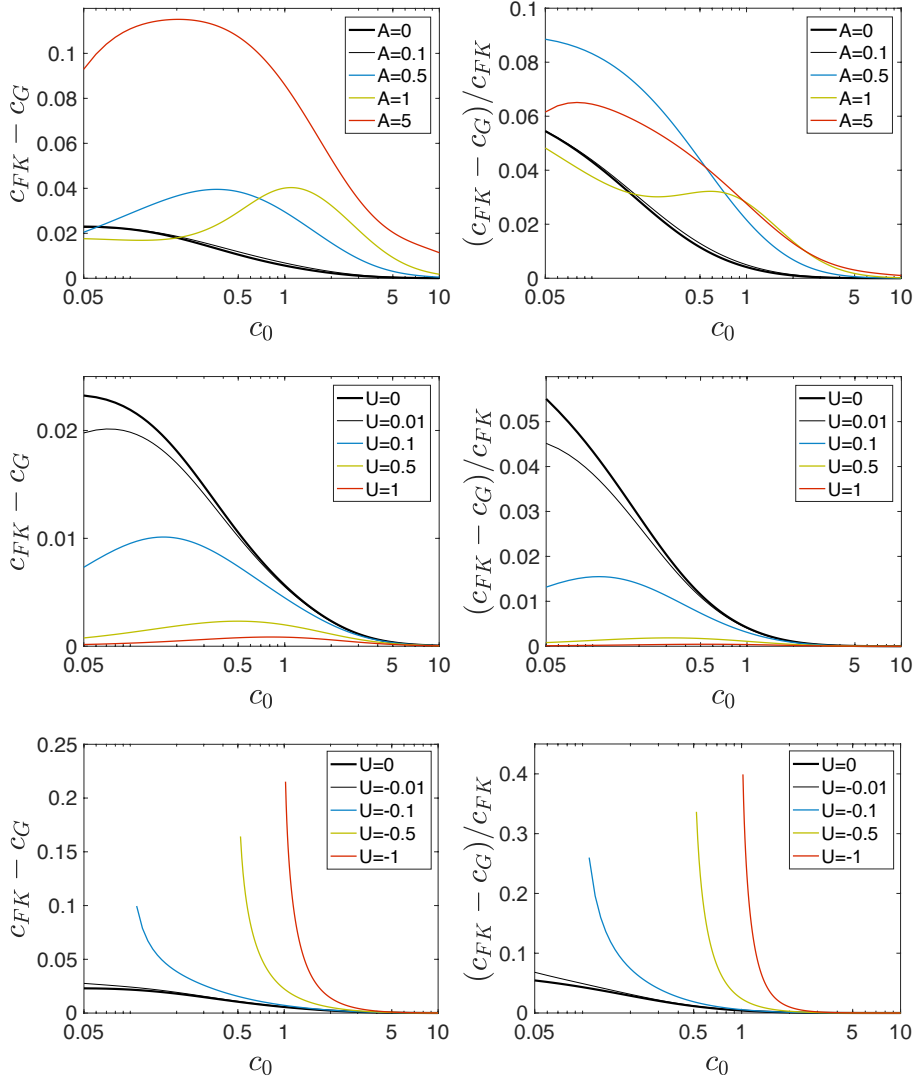
FIG. 4.5. *(Color online). Effect of the flow with streamfunction (1.8) on the (left column) difference and (right column) relative difference between the front speed c_{FK} associated with equation (FK) and the front speed c_{G} associated with equation (G). These are plotted as a function of the bare speed c_0 for (top row) various values of A with $U = 0$ and (middle and bottom rows) various values of U with $A = 0$. The values of c_{FK} and c_{G} are respectively derived from the numerical minimisation of the variational principles (3.9) and (3.12). As $c_0 \to -U > 0$, $c_{\mathrm{G}} \to 0^+$ so that the relative difference tends to 1^- (bottom right).*

give $(c_{\mathrm{FK}} - c_{\mathrm{G}})/f(A) = (1 + O(c_0^{-1}))c_0^{-3}$, where $f(A) = (16 + 538A^2 + A^4)/256$, for $c_0 \gg 1$ and $A = o(c_0)$. The relative difference between the two front speeds is shown in Figure 4.5 (top right). For the values of c_0 considered here, the maximum relative difference between c_{FK} and c_{G} corresponds to 9%, achieved for $A = 1/2$ and $c_0 = 0.05$. This is not significantly different to the maximum relative difference of 5.5% obtained for $A = 0$.

4.3. Effect of a mean flow. The behaviour of the solutions is strongly affected by the presence of a constant mean flow, when the flow contains a mixture of open and closed streamlines. We explore this by computing minimising trajectories and front speeds for $U \neq 0$ and $A = 0$. Figure 4.3 shows characteristic examples of the minimising trajectories obtained for different values of $U > 0$ (middle row) and $U < 0$ (bottom row). These trajectories are clearly invariant under the transformation $(x, y) \mapsto (-x, \pi - y)$.

For small values of c_0 and $U = O(1) > 0$, the minimising trajectories closely follow the open streamline with the maximum average horizontal speed $c_+(U)$, say, situated in the middle of the channel, which suggests that $c_{\mathrm{FK}} \sim c_+$. It can be shown that

$$(4.19) \qquad c_+(U) = \frac{2\pi}{\tau_+(U)}, \quad \text{where} \quad \tau_+(U) = 4 \int_0^{z_+} \frac{dz}{(\cos^2 z - U^2 z^2)^{1/2}}$$

and $0 \leq z_+ \leq \pi/2$ is the solution of $\cos z_+ = U z_+$. A comparison between c_{FK} and c_+ in Figure 4.4 (bottom left, inset) confirms the validity of this prediction, although convergence as $c_0 \to 0$ is slow. The prediction is not applicable when $U = O(c_0)$, however. This is because the travel time along the fastest open streamline increases (like $4 \log(1/U)$) and trajectories entering the closed streamlines (analogous to the the optimal trajectories obtained for $U = 0$ as $c_0 \to 0$) become more favourable.

For large values of c_0, we can extend the asymptotic expansion (4.12) to account for $U > 0$ to deduce that, at leading order, c_{FK} is simply shifted by U compared with its value when $U = 0$. Figure 4.4 (bottom left) confirms this behaviour by showing $c_{\mathrm{FK}} - U$ as a function of c_0 for different values of U (including $U = 0$) and exhibiting the expected collapse of curves for large c_0.

Figure 4.5 (middle row) compares the two front speeds c_{FK} and c_{G} for $U > 0$. The difference in speed decreases as U increases and is maximum for an intermediate value of c_0 for $U \neq 0$ as well as for $U = 0$. The relative difference between the two front speeds is very small: for the values of c_0 considered here, the maximum relative difference between c_{FK} and c_{G} is approximately 4.5%, achieved for $U = 0.01$ and $c_0 = 0.05$. For $U \gtrsim 0.2$, the maximum relative difference is for all values of c_0 less than 1%. When $U > 1$, the flow is entirely composed of open streamlines and therefore similar to a shear flow. As a result the two front speeds are nearly identical.

For $U < 0$ (bottom row of Figure 4.3), the mean flow opposes the right propagation of the front, and the minimising trajectories avoid regions of strong flow. For small values of c_0, they follow closely the cell boundary and differ markedly between the (FK) and (G) cases. For sufficiently small c_0, the fronts cease to propagate to the right. For (G), (3.16) indicates that there is no right-propagating front for $c_0 \leq -U - \min_x \max_y \sin x \cos y = -U$. Our numerical results suggest that right-propagating fronts do exist for all $c_0 > -U$. Figure 4.3 (bottom, left) shows the behaviour of the minimising trajectory associated with equation (G) obtained near the stationary (G) front limit for $U = -0.1$ and $c_0 = 0.11$. This is characterised by near-vertical segments at $x = 0, \pm\pi$ and $y = \pi/2$ where $\boldsymbol{u} = (-U, 0)$ and the pointwise constraint in (3.12) imposes that $\dot{x}$ be small. For (FK), right-propagating fronts are obtained for values of c_0 smaller than $-U$. For instance, for $U = -0.5$, we find a nearly stationary front, with very small (positive) c_{FK}, for $c_0 = 0.19$. The corresponding minimising trajectory is shown in Figure 4.3.

A more complete description is provided by Figure 4.4 (bottom right) which shows c_{FK} for a wide range of values of c_0, reaching close to stationary (FK) fronts as $c_{\mathrm{FK}} \to 0$

(inset). The large-c_0 leading-order behaviour of c_{FK} is the same as for $U > 0$, shifted by U compared with its value when $U = 0$. Figure 4.5 (bottom row) compares the two front speeds c_{FK} and c_{G}. Unlike the previous cases, the difference and relative difference vary monotonically with c_0, with peak values as $c_0 \to -U$ when $c_{\text{G}} \to 0$ while c_{FK} remains finite.

5. Conclusion. In this paper, we focus on the effect of spatially periodic flows on the propagation of the sharp chemical fronts that arise in the (FK) model for small diffusion and fast reaction (large Péclet and Damköhler numbers) and on their heuristic approximation by the (G) equation. We introduce a variational formulation that expresses the long-time front speed in each model in terms of periodic trajectories minimising the time of travel across a period of the flow, thus providing an alternative route to the homogenization of the corresponding Hamilton–Jacobi equations. In this formulation, the difference between the front speeds predicted by the two models arises from a different constraint imposed on the minimising trajectories. This makes it easy to deduce that the (FK) front speed is greater than or equal to the (G) front speed, with equality in the case of shear flows.

We examine the front speed for a two-parameter family of periodic cellular flows in a channel, with both zero and non-zero mean velocity U, relying on a numerical implementation of the variational representation. We find that for $U \geq 0$, the relative difference between the two front speeds is smaller than 10% for a broad range of parameters with the largest values obtained when the reactions and mean flow are both relatively weak (Da $\gtrsim 1$ number and $U \ll 1$). This is confirmed by the closed-form expressions we obtain in the two asymptotic limits $c_0 = 2\sqrt{\text{Da}/\text{Pe}} \ll 1$ and $c_0 \gg 1$. For $U < 0$, the relative difference between the two front speeds increases rapidly with decreasing c_0. As $c_0 \to -U$, the (G) front becomes stationary. There is then a range of $c_0 < -U$ for which right-propagating fronts exist for (FK) but not for (G). In this range (G) fails completely as a heuristic model for (FK) front, even at a qualitative level. The dramatic difference between the two models can be traced to the difference between the pointwise and time-integrated constraints that appear in the variational formulations (3.9) and (3.12).

A fundamental assumption that we make is that the minimising trajectories that control the two front speeds inherit the spatial periodicity of the background flow. We have carefully tested the validity of this assumption for the two-parameter family of periodic cellular flows considered here against computations over domains of length twice and three times the 2π-period of the flow and found that the minimisers are 2π periodic. These results confirm that the front speed is indeed controlled by trajectories with the same periodicity as that of the flow. It would nonetheless be desirable to establish this property rigorously. A proof would also clarify whether it is specific to the class of flows considered here or holds more generally.

We have obtained the Hamilton–Jacobi (2.3) equation for (FK) under the formal assumptions Pe $\gg 1$, Da $\gg 1$ and Da $= O(\text{Pe})$ (so that $c_0 = O(1)$). Its range of validity, and hence that of our results, is in fact much larger and includes small values of Da. This is because it is only necessary for the WKBJ approximation leading to (2.3) to hold that Pe$\nabla\mathscr{I}$ – which involves a combination of Pe and Da – be large. For shear flows, it follows from $\mathscr{I} = t\mathscr{G}(x/t, c_0) + O(1)$ and the form of $\mathscr{G}$ in (3.18) that the condition is satisfied provided that Da $\gg$ Pe^{-1}, equivalent to the requirement that the front thickness in the absence of shear be small. The situation is more complex for cellular flows because of the logarithmic dependence that arise (see (4.6)). For standard cellular flows (with $A = U = 0$), we can refer to [45] where

the asymptotic of the front speed is derived for Pe $\gg$ 1 and arbitrary Da, based on the computation of the principal eigenvalue of the relevant advection–diffusion eigenvalue problem [22, 19, 4]. It is found there that, as Da is reduced from large values, the Hamilton–Jacobi regime gives way to a different regime characterised by the scaling $\mathrm{Da} = (\log \mathrm{Pe})^{-1}$ and requiring a delicate matched-asymptotics analysis. This indicates that the results of the present paper apply for $\mathrm{Da} \gg (\log \mathrm{Pe})^{-1}$. The range of validity is presumably the same for $A \neq 0$, but not for $U \neq 0$: in the latter case, since the small-Da, i.e. small c_0 limit, is controlled by the flow around the (fastest) open streamlines, we expect the range of validity to be that of shear flows, that is, $\mathrm{Da} \gg \mathrm{Pe}^{-1}$. A complete analysis would require generalising the results of [45] to $U \neq 0$, and to deal with the subtleties that arise in the limit $U \ll 1$ (cf. the effective-diffusivity computation in this regime in [42]).

We conclude by mentioning three possible extensions of our work. The first concerns the shape of the front the (FK) model, which can be determined from the solution to Hamilton–Jacobi equation (2.3). Specifically, the front at time T is the level curve $\mathscr{I}(\boldsymbol{x}, T, c_0)$, with $\mathscr{I}(\boldsymbol{x}, T, c_0)$ defined by the variational formula in (3.2). In this case, the minimising trajectories are not periodic but satisfy the end condition $\boldsymbol{X}(T) = \boldsymbol{x}$. For large T, they stay close to the periodic trajectories determining c_{FK} for a long time interval before T, so the starting condition $\boldsymbol{X}(0) = (0, \cdot)$ can be replaced by a more practical condition that $\boldsymbol{X}(T - t)$ be asymptotic to the periodic trajectories as $t \to \infty$. The second extension concerns cellular flows in the entire plane, as opposed to the channel configuration considered in this paper. In this case, the problem is enriched by the two-dimensional nature of the front speed and the fact that minimising trajectories corresponding to speeds with irrationally related components cannot be periodic. Similarly, in the presence of a mean flow, the front speed is likely to depend sensitively on whether the two component of the flow velocity are rationally or irrationally related (the same is true for the components of the effective diffusivity tensor; see [17, 28, 34]). It would be of interest to investigate how these aspects affect the differences between c_{FK} and c_{G}. Finally, a third extension concerns other types of cellular flows. While c_{FK} remains close to c_{G} in the strong-flow regime $c_0 \ll 1$ for the 'cat's eye' flow (obtained by a periodic variation to the basic cellular flow [39]), the difference can become significant for the (integrable) three-dimensional Roberts cellular flow [51]. For more complex (non-integrable) flows, e.g. the time-periodic, two-dimensional cellular flows considered in [5] or the three-dimensional Arnold–Beltrami–Childress flows [11], the situation is more challenging [31]. These flows could be tackled by the analytic and numerical approaches employed in this paper. We leave this for future work.

Appendix A. Numerical procedure. For (FK), we focus on the variational expression (3.5) and approximate the periodic trajectory $\boldsymbol{X}(t)$ by a piecewise linear function $\boldsymbol{X}_d$, defined on an evenly spaced time grid $\{t_l = l\Delta t\}_{l=0}^{N}$ where $t_N = \tau$. The action functional in (3.5) is approximated by the sum

$$(\text{A.1}) \qquad G_d(\{\boldsymbol{X}_l\}_{l=0}^{N}, c_0) = \frac{1}{4}\left(\frac{1}{\tau}\sum_{l=0}^{N-1} L_d(\boldsymbol{X}_l, \boldsymbol{X}_{l+1}) - c_0^2\right),$$

where $\boldsymbol{X}_l = \boldsymbol{X}_d(l\Delta t)$ approximates $\boldsymbol{X}(t_l)$,

$$(A.2) \qquad L_d(\boldsymbol{X}_l, \boldsymbol{X}_{l+1}) = \Delta t \mathscr{L}\left(\frac{\boldsymbol{X}_{l+1} - \boldsymbol{X}_l}{\Delta t}, \frac{\boldsymbol{X}_l + \boldsymbol{X}_{l+1}}{2}\right),$$

with $\mathscr{L}$ is defined (3.1), and we have used a midpoint rule to approximate the integral. The symplectic nature of the midpoint rule (e.g. [30]) ensures that the corresponding value of the Hamiltonian remains constant over time.

For (G), we focus on the variational expression (3.14). Calculations are easiest taking $\Theta(x)$ to parameterise the pointwise constraint in polar coordinates yielding

$$(A.3a) \qquad T'(x) = \frac{1}{(u(x, Y(x)) + c_0 \cos \Theta(x))},$$

$$(A.3b) \qquad Y'(x) = \frac{u(x, Y(x)) + c_0 \cos \Theta(x)}{v(x, Y(x)) + c_0 \sin \Theta(x)},$$

where $\Theta(x + 2\pi) = \Theta(x)$. We now approximate $Y(x)$, $\Theta(x)$ and $T(x)$ by piecewise linear functions Y_d, Θ_d and T_d, defined on an evenly spaced spatial grid $\{x_k = k\Delta x\}_{k=0}^{N}$ where $x_N = 2\pi$. The total time period τ may then be approximated as

$$(A.4a) \qquad \tau_d(\{Y_k, \Theta_k\}_{k=0}^{N}) = \sum_{k=0}^{N-1} T_{k+1} - T_k \ \text{ where } \ T_{k+1} - T_k \approx \int_{k\Delta x}^{(k+1)\Delta x} T'(x)\mathrm{x}$$

subject to the constraint

$$(A.4b) \qquad Y_{k+1} - Y_k \approx \int_{k\Delta x}^{(k+1)\Delta x} Y'(x)\mathrm{x}, \quad \text{for } k = 1 \ldots N.$$

Here, $Y_k = Y_d(k\Delta x)$, $\Theta_k = \Theta_d(k\Delta x)$ and $T_k = T_d(k\Delta x)$ are respectively an approximation to $Y(x_k)$, $\Theta(x_k)$ and $T(x_k)$. We use the midpoint rule to approximate the integrals in (A.4) so that

$$(A.5a) \qquad T_{k+1} - T_k = \Delta x \frac{1}{u\left(x_k + \frac{1}{2}\Delta x, \frac{1}{2}(Y_{k+1} + Y_k)\right) + c_0 \cos\left(\frac{1}{2}(\Theta_{k+1} + \Theta_k)\right)}$$

and

$$(A.5b) \qquad Y_{k+1} - Y_k = \Delta x \frac{u\left(x_k + \frac{1}{2}\Delta x, \frac{1}{2}(Y_{k+1} + Y_k)\right) + c_0 \cos\left(\frac{1}{2}(\Theta_{k+1} + \Theta_k)\right)}{v\left(x_k + \frac{1}{2}\Delta x, \frac{1}{2}(Y_{k+1} + Y_k)\right) + c_0 \sin\left(\frac{1}{2}(\Theta_{k+1} + \Theta_k)\right)}.$$

In both problems, we use MATLAB's Symbolic Math Toolbox to express the trajectories, action functional and constraints in symbolic form. We then take $\Delta t = \tau/200$ and $\Delta x = \pi/100$ and use MATLAB's Optimization Toolbox to find the optimal trajectories that minimise the value of (i) $T_d(\{Y_k, \Theta_k\}_{k=0}^{N})$ from where we obtain τ_{G} as a function of c_0 and (ii) $G_d(\{X_l, Y_l\}_{l=0}^{N}, c_0)$ from where we solve $\mathscr{G}(c, c_0)$. We then use (2.10) to deduce c_0 for a given c_{FK}. The advantage of symbolic calculations is that the gradient vectors of the discretised action functional and constraints can readily be determined. These are necessary to increase the accuracy and efficiency of the optimisation solver.

The computations need a good first guess to be initialised. For problem (3.12), we use the large-c_0 asymptotic behaviour of the trajectory obtained for the basic

cellular flow with closed streamlines ($A = U = 0$) given by equation (4.18). We then iterate over a range of values of c_0 using the previously determined trajectory as an initial guess to find the next minimiser. Similarly, for problem (3.9) we use the large-c asymptotic behaviour of the trajectory given by equation (4.15). The iteration is this time taking place over a range of values of c_{FK}. The same solutions are used as first guess to obtain the optimal solutions for a range of A and U values.

REFERENCES

[1] M. Abel, M. Cencini, D. Vergni, and A. Vulpiani, *Front speed enhancement in cellular flows*, Chaos, 12 (2002), pp. 481–488.

[2] B. Audoly, H. Berestycki, and Y. Pomeau, *Réaction diffusion en écoulement stationnaire rapide*, C. R. Acad. Sci. Paris, t. 328, Série II b, 328 (2000), pp. 255–262.

[3] D. Bargteil and T. Solomon, *Barriers to front propagation in ordered and disordered vortex flows*, Chaos, 22 (2012), p. 037103.

[4] H. Berestycki and F. Hamel, *Front propagation in periodic excitable media*, Comm. Pure Appl. Math., 55 (2002), pp. 949–1032.

[5] R. Camassa and S. Wiggins, *Chaotic advection in a rayleigh-bénard flow*, Phys. Rev. A, 43 (1991), pp. 774–797.

[6] P. Cardaliaguet, J. Nolen, and P. E. Souganidis, *Homogenization and enhancement for the G-equation*, Arch. Ration. Mech. Anal., 199 (2011), pp. 527–561.

[7] P. Cardaliaguet and P. E. Souganidis, *Homogenization and enhancement of the G-equation in random environments*, Comm. Pure Appl. Math, 66 (2013), pp. 1582–1628.

[8] M. Cencini, A. Torcini, D. Vergni, and A. Vulpiani, *Thin front propagation in steady and unsteady cellular flows*, Phys. Fluids, 15 (2003), pp. 679–688.

[9] R. Courant and D. Hilbert, *Methods of Mathematical Physics*, Wiley, New York, 1991.

[10] *NIST Digital Library of Mathematical Functions*. http://dlmf.nist.gov/, Release 1.0.15 of 2017-06-01. F. W. J. Olver, A. B. Olde Daalhuis, D. W. Lozier, B. I. Schneider, R. F. Boisvert, C. W. Clark, B. R. Miller and B. V. Saunders, eds.

[11] T. Dombre, U. Frisch, J. M. Greene, M. Hnon, A. Mehr, and A. M. Soward, *Chaotic streamlines in the abc flows*, Journal of Fluid Mechanics, 167 (1986), p. 353?391.

[12] M. El Smaily and S. Kirsch, *The speed of propagation for kpp reaction-diffusion equations within large drift*, Adv. Differential Equations, 16 (2011), pp. 361–400.

[13] P. F. Embid, A. J. Majda, and P. E. Souganidis, *Comparison of turbulent flame speeds from complete averaging and the gequation*, Phys. Fluids, 7 (1995), p. 2052.

[14] L. C. Evans, *Periodic homogenisation of certain fully nonlinear partial differential equations*, Proc. R. Soc. Edin. A, 120 (1992), pp. 245–265.

[15] L. C. Evans, *Partial Differential Equations*, vol. 19, American Mathematical Society, 2010.

[16] L. C. Evans, P. E. Souganidis, G. Fournier, and M. Willem, *A PDE approach to certain large deviation problems for systems of parabolic equations*, Ann. I. H. Poincare-An., S6 (1989), pp. 229–258.

[17] A. Fannjiang and G. C. Papanicolaou, *Convection enhanced diffusion for periodic flows*, SIAM J. Appl. Math., 54 (1994), pp. 333–408.

[18] R. Fisher, *The wave of advance of advantageous genes*, Ann. Eugenics, 7 (1937), pp. 355–369.

[19] M. I. Freidlin, *Functional Integration and Partial Differential Equations*, Princeton University Press, 1985.

[20] M. I. Freidlin and R. B. Sowers, *A comparison of homogenization and large deviations, with applications to wavefront propagation*, Stoch. Proc. Appl., 82 (1999), pp. 23 – 52.

[21] M. I. Freidlin and A. D. Wentzell, *Random perturbations of dynamical systems*, Springer, 1984.

[22] J. Gärtner and M. I. Freidlin, *On the propagation of concentration waves in periodic and random media.*, Soviet Math. Dokl., 20 (1979), pp. 1282–1286.

[23] A. R. Kerstein, W. T. Ashurst, and F. A. Williams, *Field equation for interface propagation in an unsteady homogeneous flow field*, Phys. Rev. A, 37 (1988), pp. 2728–2731.

[24] B. Khouider and A. Bourlioux, *Computing the effective Hamiltonian in the Majda–Souganidis model of turbulent premixed flames*, SIAM J. Num. Anal., 40 (2002), pp. 1330–1353.

[25] A. N. Kolmogorov, I. G. Petrovsky, and N. S. Piskunov, *Étude de l'équation de la diffusion avec croissance de la quantité de matière et son application à un problème biologique*, Bull. Univ. Moskov. Ser. Internat. Sect., 1 (1937), pp. 1–25.

[26] P. L. LIONS, G. C. PAPANICOLAOU, AND S. VARADHAN, *Homogenization of Hamilton–Jacobi equations.* (unpublished).

[27] J. R. MAHONEY, J. LI, C. BOYER, T. SOLOMON, AND K. A. MITCHELL, *Frozen reaction fronts in steady flows: A burning-invariant-manifold perspective*, Phys. Rev. E, 92 (2015), p. 063005.

[28] A. J. MAJDA AND P. R. KRAMER, *Simplified models for turbulent diffusion: Theory, numerical modelling, and physical phenomena*, Phys. Rep., 314 (1999), pp. 237 – 574.

[29] A. J. MAJDA AND O. E. SOUGANIDIS, *Large-scale front dynamics for turbulent reaction–diffusion equations with separated velocity scales*, Nonlinearity, 7 (1994), pp. 1–30.

[30] J. E. MARSDEN AND M. WEST, *Discrete mechanics and variational integrators*, Acta Numer., 10 (2001), p. 357514.

[31] T. MCMILLEN, J. XIN, Y. YU, AND A. ZLATOS, *Ballistic orbits and front speed enhancement for abc flows*, SIAM J. Appl. Dyn. Syst., 15 (2016), pp. 1753–1782.

[32] P. W. MEGSON, M. L. NAJARIAN, K. E. LILIENTHAL, AND T. H. SOLOMON, *Pinning of reaction fronts by burning invariant manifolds in extended flows*, Phys. Fluids, 27 (2015), p. 023601.

[33] Z. NEUFELD AND E. HERNÁNDEZ-GARCIA, *Chemical and Biological Processes in Fluid Flows: A Dynamical Systems Approach*, Imperial College Press, 2009.

[34] G. A. PAVLIOTIS AND A. M. STUART, *Multiscale Methods: Averaging and Homogenization*, Springer, 2007.

[35] N. PETERS, *Turbulent combustion*, Cambridge University Press, 2000.

[36] A. PIATNITSKI, *Asymptotic behaviour of the ground state of singularly perturbed elliptic equations*, Commun. Math. Phys., 197 (1998), pp. 527–551.

[37] A. POCHEAU AND F. HARAMBAT, *Front propagation in a laminar cellular flow: Shapes, velocities, and least time criterion*, Phys. Rev. E, 77 (2008), p. 036304.

[38] G. O. ROBERTS, *Dynamo action of fluid motions with two-dimensional periodicity*, Phil. Trans. R. Soc. London Ser. A, 271 (1972), pp. 411–454.

[39] S. S. CHILDRESS AND A. M. SOWARD, *Scalar transport and alpha-effect for a family of cat's-eye flows*, J. Fluid Mech., 205 (1989), pp. 99–133.

[40] M. E. SCHWARTZ AND T. H. SOLOMON, *Chemical reaction fronts in ordered and disordered cellular flows with opposing winds*, Phys. Rev. Lett., 100 (2008), p. 028302.

[41] J. A. SETHIAN, *Curvature and the evolution of fronts*, Comm. Math. Phys., 101 (1985), pp. 487–499.

[42] A. M. SOWARD AND S. CHILDRESS, *Large magnetic Reynolds number dynamo action in a spatially periodic flow with mean motion*, Phil. Trans. R. Soc. London Ser. A, 331 (1990), pp. 649–733.

[43] T. TEL, A. DE MOURA, C. GREBOGI, AND G. KÁROLYI, *Chemical and biological activity in open flows: A dynamical systems approach*, Phys. Rep., 413 (2005), pp. 91–196.

[44] A. TZELLA AND J. VANNESTE, *Front propagation in cellular flows for fast reaction and small diffusivity*, Phys. Rev. E, 90 (2014), p. 011001.

[45] A. TZELLA AND J. VANNESTE, *FKPP fronts in cellular flows: The Large-Péclet regime*, SIAM J. Appl. Math., 75 (2015), pp. 1789–1816.

[46] F. A. WILLIAMS, *The Mathematics of Combustion*, SIAM, 1985.

[47] J. XIN, *Existence and nonexistence of traveling waves and reaction-diffusion front propagation in periodic media*, J. Stat. Phys., 73 (1993), pp. 893–926.

[48] ———, *Front propagation in heterogeneous media*, SIAM Rev., 42 (2000), pp. 161–230.

[49] J. XIN AND Y. YU, *Periodic homogenization of the inviscid G-equation for incompressible flows*, Commun. Math. Sci., 8 (2010), pp. 1067–1078.

[50] J. XIN AND Y. YU, *Sharp asymptotic growth laws of turbulent flame speeds in cellular flows by inviscid Hamilton–Jacobi models*, Ann. I. H. Poincaré AN, 30 (2013), pp. 1049 – 1068.

[51] J. XIN AND Y. YU, *Asymptotic growth rates and strong bending of turbulent flame speeds of g-equation in steady two-dimensional incompressible periodic flows*, SIAM J. Math. Analysis, 46 (2014), pp. 2444–2467.